Research Article

Magnetic plasmon induced transparency in three-dimensional metamolecules

Pin Chieh Wu[1], Wei Ting Chen[1], Kuang-Yu Yang[1], Chih Ting Hsiao[2], Greg Sun[3], Ai Qun Liu[4], Nikolay I. Zheludev[5] and Din Ping Tsai[1,2,6,*]

[1] Graduate Institute of Applied Physics, National Taiwan University, Taipei 10617, Taiwan,
e-mail: dptsai@phys.ntu.edu.tw
[2] Department of Physics, National Taiwan University, Taipei 10617, Taiwan
[3] Department of Physics, University of Massachusetts Boston, MA 02125, USA
[4] School of Electrical and Electronic Engineering, Nanyang Technological University, 639798, Singapore
[5] Optoelectronics Research Centre and Centre for Photonic Metamaterials, University of Southampton, Southampton SO17 1BJ, UK
[6] Research Center for Applied Sciences, Academia Sinica, Taipei 11529, Taiwan

*Corresponding author

Abstract

In a laser-driven atomic quantum system, a continuous state couples to a discrete state resulting in quantum interference that provides a transmission peak within a broad absorption profile the so-called electromagnetically induced transparency (EIT). In the field of plasmonic metamaterials, the sub-wavelength metallic structures play a role similar to atoms in nature. The interference of their near-field coupling at plasmonic resonance leads to a plasmon induced transparency (PIT) that is analogous to the EIT of atomic systems. A sensitive control of the PIT is crucial to a range of potential applications such as slowing light and biosensor. So far, the PIT phenomena often arise from the electric resonance, such as an electric dipole state coupled to an electric quadrupole state. Here we report the first three-dimensional photonic metamaterial consisting of an array of erected U-shape plasmonic gold nanostructures that exhibits PIT phenomenon with magnetic dipolar interaction between magnetic metamolecules. We further demonstrate using a numerical simulation that the coupling between the different excited pathways at an intermediate resonant wavelength allows for a π phase shift resulting in a destructive interference. A classical *RLC* circuit was also proposed to explain the coupling effects between the bright and dark modes of EIT-like electromagnetic spectra. This work paves a promising approach to achieve magnetic plasmon devices.

Keywords: metamaterials; plasmon induced transparency; magnetic resonance.

Introduction

Plasmonic metamaterials are composed of artificial metamolecules exhibiting unusual optical properties such as negative refraction index [1, 2], and toroidal dipolar response [3, 4] that can lead to applications that are otherwise unattainable in nature, such as sub-diffraction imaging [5, 6], and optical and spectrum manipulation [7–10]. These unique characteristics also enable us to explore tunability and nonlinearity that either do not exist in nature or are too weak for practical applications [11, 12]. The magnetic and electric responses of artificial metamolecules play a similar role to those of atoms in electromagnetic media. Split ring resonators (SRRs), commonly constructed building blocks of plasmonic metamaterials, have been proposed to produce electric as well as magnetic dipolar response [13–16]. The dipolar response of such SRR structures can be excited by an incident wave with either electric field perpendicular to two prongs or the magnetic field passing through the gap of SRR [15]. While the electric dipolar response can be readily explored, the magnetic counterpart has proven to be much harder to excite because of the orientation in induced magnetic dipoles of planar SRRs, which has largely prevented a number of important applications that rely upon magnetic interactions [17, 18]. This limitation can be overcome with SRR structures arranged in a particular orientation that enables magnetic dipolar interaction between neighboring SRRs for a specific incident wave [14, 16, 19–21].

Electromagnetically induced transparency (EIT) is a quantum interference effect in a material between two pathways induced by two different incident lasers [22, 23]. By introducing a pumping laser to the material, the absorption intensity of the probe laser can be dramatically reduced, producing a controllable transparency window in electromagnetic spectra. Many electromagnetic theorems and classical models such as mass-spring systems and RLC circuits were used to analyze the mechanism of EIT [24–27]. Such a phenomenon has also been observed in plasmonic metamaterials where plasmon induced transparency (PIT) works very similarly to that of EIT, except that in the case of PIT, the mechanism is considered as the plasmon coupling of the different pathways of metamolecules between a bright element (radiative mode, which can couple to incident light) and a dark element (subradiative mode, which can hardly couple to incident light) which leads to sharp resonance and suppresses the radiative loss [28]. Therefore, PIT provides a promising pathway towards realizing of ultra-sensitive biosensors [29, 30], slow light propagation [31, 32], and nanoruler of sub-microstructures or bio-molecular [33, 34].

Up to now, due to fabrication limitation [35, 36], most plasmonic metamaterials exhibiting PIT have been demonstrated in planar or multi-layered structures by electric coupling rather than by magnetic coupling [28, 30, 37–40]. Recently,

a number of plasmonic structures with magnetic resonances have also been proposed because of their potential advantages [41, 42]. For example, Liu et al. demonstrated the propagation of electromagnetic energy via magnetic plasmons is capable of supporting low-loss propagation of plasmon modes [17, 43]. The utilization of magnetic coupling will provide an additional degree of design freedom for plasmonic devices based on magnetic plasmon material.

In this paper, we numerically and experimentally demonstrate the first PIT phenomenon in three-dimensional U-shaped SRR metamolecules in the optical region. The PIT is created by the magnetic resonance where the dark mode is excited through coupling with the bright mode via magnetic dipolar response using the broken geometrical symmetry. The transmittance intensity at the PIT peak can be controlled precisely with the manipulation of structural symmetry. We find that the coupling strength between the bright and dark modes has a direct relationship with the degree and broadness of the transparency window in transmittance spectra. Using numerical simulation, we demonstrate the π phase shift between the different excitation paths, providing a clear evidence of the destructive interference at the PIT peak. Finally, we develop a coupled circuit to explain the coupling strength between the different elements in a unit cell.

Materials and methods

Using the electron beam double exposure process with alignment technology [19], we fabricated three erected U-shaped gold resonance rings in a unit cell covering a total area of 75×75 μm^2 on fused silica. For precision alignment of the e-beam double exposure process, two golden cross alignment marks (size 9×150 μm) with 100 nm thickness were first fabricated. A 200 nm-thick PMMA layer was spin-coated at 4000 rpm on fused silica wafer and then baked on a hot plate for 3 min at 180°C. The Espacer (Kokusai Eisei Co., Showa Denso Group, Japan) is spin-coated at 1500 rpm over the PMMA layer. Espacer is an organic polymer which can eliminate the static charging problem during the e-beam exposure process. An ELS-7000 electron beam lithography system (Elionix Inc., Tokyo, Japan) at the acceleration voltage of 100 keV with 30 picoamp (pA) of current is used for exposure. The bottom rods of erected SRR structures were defined in positive resist (495k PMMA) after the first e-beam exposure and lift-off process. Subsequently, the two prongs of erected SRR structure are made by second e-beam exposure and lift-off process.

All of the transmittance spectra were measured using the VERTEX 70 Fourier-transform infared spectrometer (Bruker Co., Ettlingen, Germany) with a Bruker HYPERION 1000 infrared microscope (15× Cassegrain objective, numerical aperture NA=0.4, near-infrared polarizer, and an InGaAs detector). An iris was used to collect the incident light to a square area of about 75×75 μm^2.

Results and discussions

The geometries of a three-dimensional plasmonic metamolecule are illustrated in Figure 1A along with the
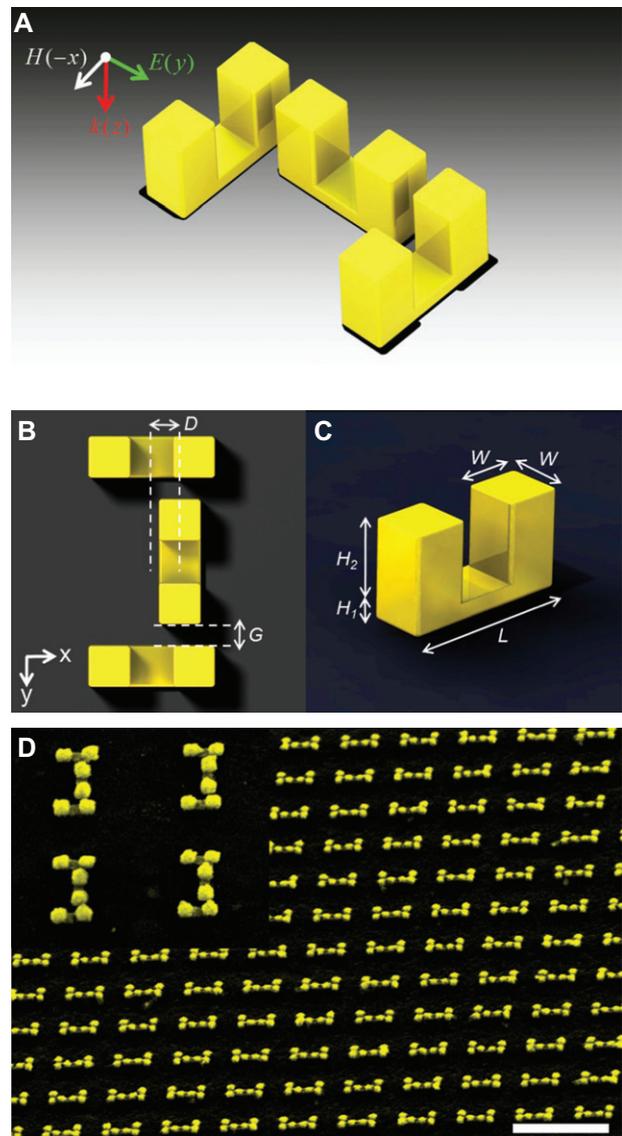
Figure 1 (A) Schematic diagram of a single SRR metamolecule unit cell. Each unit cell consisted of three erected gold SRRs with 600 nm period in both x and y directions. The optical properties of such metamolecule are studied in the case of y-polarized illumination. (B) Top view of the metamolecule with G is 30 nm and definition of the displacement parameter D. (C) The feature size of a single SRR structure: H_1=30 nm, H_2=80 nm, W=60 nm and L=180 nm, respectively. (D) Oblique view of SEM image of the fabricated metamolecules array while distance parameter D is 30 nm. Insets: zoom in image. The scale bar is 1 μm.

polarization state of an incident light. The metamolecule (unit cell) consists of three erected U-shaped gold split-ring resonators, including one in the middle along the vertical direction (VSRR) and a pair on the side along the horizontal direction (HSRR). The gap G between the VSRR and HSRR is fixed at 30 nm and the lateral displacement between the central axes of VSRR and HSRR pair is defined as D (see Figure 1B). The feature sizes of each single SRR structure is presented in Figure 1C. The VSRR, supports a bright mode whose magnetic resonance can be excited by a normal incident light

with electric field polarization along the y direction. Owing to the strong coupling between the incident light and VSRR, the bright mode suffers a significant far field scattering loss. On the contrary, the HSRR pair supporting only dark modes can be viewed as non-radiative elements because of its much weaker coupling with the incident light. The coupling effect between the incident light, VSRR and HSRR can be studied by introducing asymmetry between the SRRs with the tuning of the displacement parameter D.

In order to investigate the coupling effects between VSRR and HSRRs, we fabricated three different kinds of meta-molecules corresponding to displacement parameters $D=0$ nm, 30 nm, and 60 nm. Figure 1D presents oblique views in the case of $D=30$ nm, showing the accurate alignment for the fabrication process (the misalignment is controlled to within 10 nm). To experimentally investigate the optical properties of these PIT metamolecules, near-infrared transmittance spectra are measured by Fourier-transform infrared spectrometer in the case of normal illumination with the magnetic field passing through the gap of middle SRR. The measured transmittance spectra are presented by colored curves in Figure 2. In the case of $D=0$ nm (dark yellow line in Figure 2), a typical transmittance profile with a maximum power absorption can be observed. The origin of this plasmonic resonance is contributed by the magnetic resonance of VSRR (we will present a more detailed analysis on this in the next section). By introducing structural asymmetry with $D=30$ nm (blue line in Figure 2), a transmittance peak appears within the resonance profile of $D=0$ nm case as a result of the near-field coupling between VSRR and HSRRs. Furthermore, the transmittance peak becomes more pronounced for $D=60$ nm (orange line in Figure 2).

Now, we present numerical simulation results for the various coupling effects in the plasmonic metamolecule unit cells. All of the simulation spectra and field distribution are carried out by solving the three-dimensional Maxwell equation with the commercial COMSOL Multiphysics software based on the finite element method (FEM). A single metamolecule pattern was simulated (with periodic boundary conditions) under normal-incidence illumination by linearly-polarized light in the wavelength range from 950 nm to 1750 nm. The refractive index of fused silica wafer is fixed at 1.4584. The permittivity of bulk gold in the near infrared regime is described by the Drude-Lorentz model with plasmon frequency ω_p=8.997 eV and damping constant Γ_p=0.14 eV. The simulation results are calculated using a damping constant that is two times larger than the bulk value because of the surface defect scattering and grain effects. Figure 3 shows the simulation transmittance (Figure 3A), absorbance (Figure 3B) as a function of incident wavelength, and the magnetic field intensity (Figure 3C) for the three cases: $D=0$ nm, 30 nm and 60 nm. The absorbance spectra were performed using $A=1-T-R$, where R is reflectance. All the simulation results are in qualitative agreement with our experiment, i.e. the structural asymmetry allows for the excitation of the dark modes which are otherwise not allowed to be excited, resulting in PIT spectra. The small difference between our experimental and simulation results is likely to arise from the deviation of fabricated patterns from that of
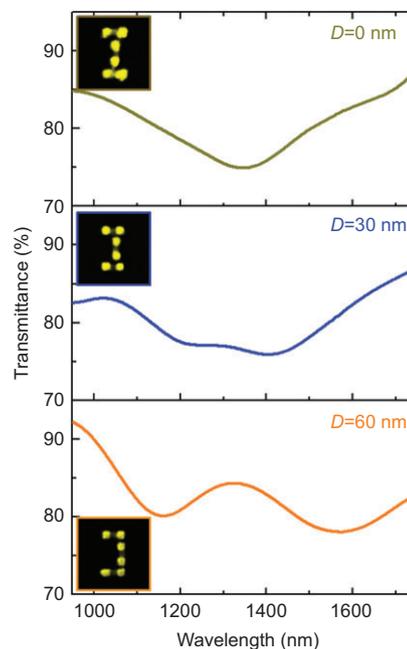
Figure 2 The experimental transmittance spectra upon varying distance parameter D. The evolution of the PIT features in the electromagnetic spectra show a strong dependence on the distance parameter. All the insets show the top-view SEM images of the corresponding samples.

the simulation design as well as the fact that the sample surface is not as smooth as the simulation condition. Therefore, there is a slight difference compared with the simulation (Figure 3A) and measured (Figure 2) transmittance spectra.

Similarly, in the case of $D=0$ nm, due to the plasmonic resonance of the VSRR at the middle of metamolecule unit cell, a single transmittance dip can be observed. The plasmonic resonance of VSRR shows a strong magnetic dipolar response resulting from a ring-like current oscillation on the surface of VSRR. The schematic of the magnetic field lines for the induced magnetic dipole of VSRR is shown in the inset of Figure 3A. In this case, the HSRRs cannot be excited either by the y-polarized incident light or indirectly by the induced magnetic dipole of VSRR, since the VSRR induced magnetic field is parallel to the gap of HSRRs. By introducing structural asymmetry with $D=30$ nm, a transmittance peak appears (see the second row of Figure 3) within the resonance profile for $D=0$ nm. It reveals that increasing structural asymmetry will enhance the coupling effect between the VSRR and HSRR pair. The structural asymmetry, allows for a component of the magnetic field induced by the plasmonic resonance of VSRR to pass through the gap of HSRRs. Subsequently, according to Lenz's law, an additional magnetic field will be induced in the HSRR pair to oppose the change of magnetic flux going through their gaps, resulting in the magnetic resonance of HSRRs. It is worth mentioning that the VSRR induced current oscillations in the two HSRRs are opposite (magnetic quadrupole) of each other (see the purple arrows of the direction of magnetic field in Figure 3C). As a result, the HSRRs supporting only dark modes exhibit a higher quality factor than
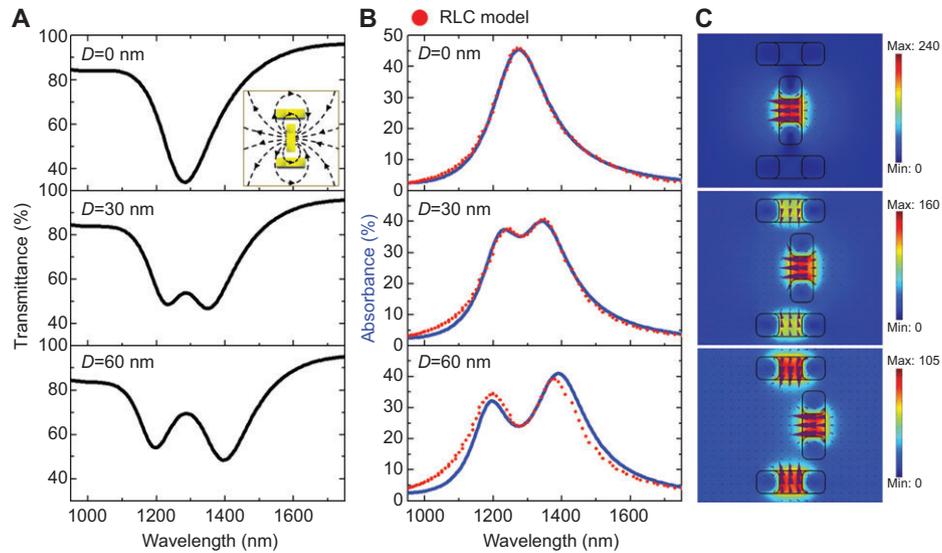
Figure 3 (A) Simulation transmittance spectra for y-polarized illumination in the case of D=0 nm, 30 nm, and 60 nm, respectively. The inset shows the schematic magnetic field lines of an induced magnetic dipole of VSRR. (B) Simulation absorbance spectra for y-polarized illumination in the case of D=0 nm, 30 nm, and 60 nm, respectively. The red-dotted lines represent the fitting curves calculated from Eq. (5). (C) Simulation results of magnetic field intensity in arbitrary units (color-coded) and direction of magnetic field (purple arrows) in different distance parameter D.

that of VSRR (bright mode) because the scattering power of the induced magnetic dipoles in the HSRRs will cancel each other out. The PIT phenomenon is very difficult to observe without the high quality factor of the dark mode even when the coupling between bright and dark modes is strong. The high quality factor of the HSRRs contributes to the fact that we were able to observe and simulate a sharp transmittance peak for the case of D = 60 nm.

There are two different coupling pathways between incident light and our metamolecules. In order to investigate the phase relation between two excited pathways, the oscillating magnitude of induced magnetic field for both VSRR and HSRRs have been calculated and carried by FEM simulation. Figure 4A shows the schematic diagram (top view) with the direction of magnetic field Hx and Hy for D=60 nm. The magnitudes of induced magnetic field in x-component Hx (green arrow
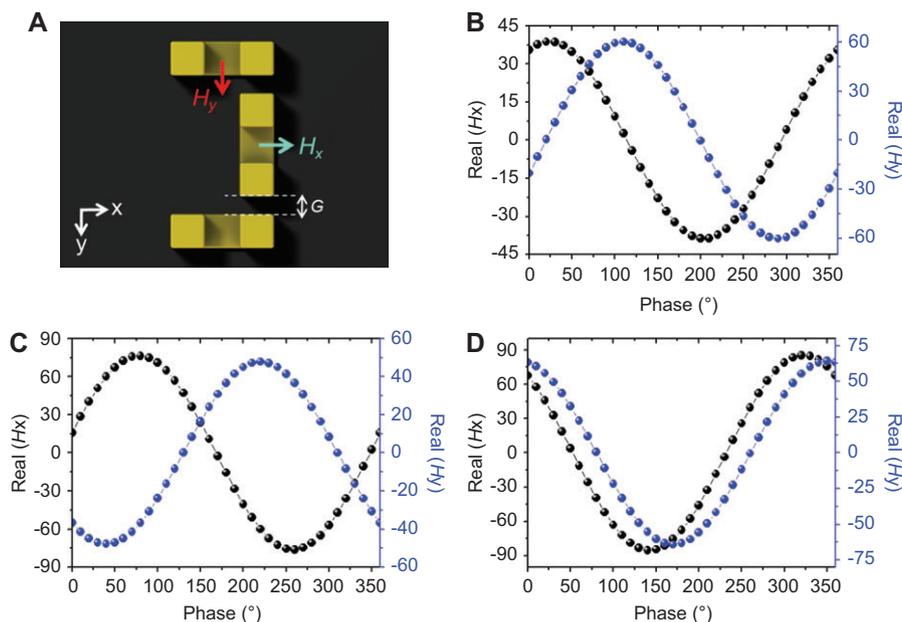
Figure 4 (A) The schematic diagram of PIT structure in the case of D=60 nm and G=30 nm. The Hx response and Hy response are detected at the middle point of resonant ring (position indicated by a green arrow and a red arrow). Real part of magnetic field components Hx and Hy as a function of phase variation for incident wavelength (B) λ=1285 nm (C) 1195 nm and (D) 1395 nm, respectively, extracted by FEM simulation.

in Figure 4A) and y-component Hy (red arrow in Figure 4A) are extracted from the middle point of VSRR and HSRRs, respectively. Figures 4B–D show the phase revolution corresponding to Hx and Hy at wavelength λ=1285 nm, 1195 nm and 1395 nm, respectively. We find a 90° phase shift between the induced magnetic field of VSRR with respect to that of HSRR at wavelength λ=1285 nm (Figure 4B). We define the oscillating phase at the first excitation pathway (|*Incident light*⟩→|*VSRR*⟩) to be zero due to the excitation of VSRR under normal illumination. Because of the near-field coupling between VSRR and HSRRs, the second excitation pathway (|*Incident light*⟩→|*VSRR*⟩→|*HSRRs*⟩→|*VSRR*⟩) experiences a 180° phase delay as the excited HSRRs couples energy back to the VSRR resulting from $\pi/2$ phase shift between VSRR and HSRRs. As a result, a 180° phase shift between the first and second pathway leads to the destructive interference that results in a transmission peak at wavelength λ=1285 nm, similar to the EIT phenomenon in atomic physics [23]. On the other hand, the phase shift between VSRR and HSRRs is 140° and 30° at wavelength λ=1195 nm and 1395 nm, respectively, as shown in Figures 4C and 4D. It reveals that the transmittance spectra exhibit visible dips rather than peaks without a 180° phase shift between two excited pathways.

For investigating the contribution of magnetic and magneto-electric coupling effect between VSRR and HSRRs, the enhancement of scattered power is calculated, as shown in Figure 5. The magnitude of the scattered power of electric and magnetic multipoles can be defined as [3, 4]:

electric dipole moment:
$$\mathbf{P}=\frac{1}{i\omega}\int \mathbf{j}d^3r, \tag{1}$$

magnetic dipole moment:
$$\mathbf{M}=\frac{1}{2c}\int (\mathbf{r}\times\mathbf{j})d^3r, \tag{2}$$

electric quadrupole moment:
$$Q_{\alpha\beta}=\frac{1}{i2\omega}\int\left[r_\alpha j_\beta+r_\beta j_\alpha-\frac{2}{3}(\mathbf{r}\cdot\mathbf{j})\delta_{\alpha\beta}\right]d^3r, \tag{3}$$

magnetic quadrupole moment:
$$M_{\alpha\beta}=\frac{1}{3c}\int\left[(\mathbf{r}\times\mathbf{j})_\alpha r_\beta+(\mathbf{r}\times\mathbf{j})_\beta r_\alpha\right]d^3r, \tag{4}$$

where c is the speed of light, j is the induced volume current density and α, β = x, y, z. Subsequently, the scattered power of the multipole moments is calculated from the induced currents [3, 4]:

$$I=\frac{2\omega^4}{3c^3}|\mathbf{P}|^2+\frac{2\omega^4}{3c^3}|\mathbf{M}|^2+\frac{\omega^6}{5c^5}\sum|Q_{\alpha\beta}|^2+\frac{\omega^6}{40c^5}\sum|M_{\alpha\beta}|^2+O\left(\frac{1}{c^5}\right), \tag{5}$$

The scattered power enhancement is defined as $\dfrac{(Scattered\ power)_{D=30\ nm}}{(Scattered\ power)_{D=0\ nm}}$ (Figure 5A) and

$\dfrac{(Scattered\ power)_{D=60\ nm}}{(Scattered\ power)_{D=0\ nm}}$ (Figure 5B), respectively.

The larger scattered power enhancement indicates the stronger allowance of exciting multipole while structural symmetry is broken. In Figure 5, the magnetic dipole as well as the electric multipoles show weaker enhancement of scattered power. On the contrary, the scattered power enhancement of magnetic quadrupoles is much larger than that of the electric multipole as introducing the structural asymmetry. These results indicate a magnetic quadrupole can actually be excited in the absence of structural symmetry giving rise to the larger scattered power of magnetic quadrupole. As a result, the magnetic dipole-quadrupole interaction plays a dominant role in this PIT metamolecule.

To provide a quantitative analysis of the PIT phenomena, we describe the coupling mechanism using a model of three coupled RLC circuits (see Figure 6A). The VSRR is described by the first circuit driven by $V_{in}(t) = Ve^{-i\omega t}$ which describes the in-coupling effect of the incident light. The HSRRs, on the other hand, can be excited via the induced magnetic field of VSRR, thus the coupling mechanism between the first circuit and other two circuits is accounted for as mutual inductance M_{21} and M_{31}. With the identical geometric dimensions of the three SRRs inside a metamolecule unit cell, their inductance and capacitance are set as equal $L_1=L_2=L_3=L$ and $C_1=C_2=C_3=C$. The Lagrangian of the coupled circuit system can be written as

$$\Gamma=\frac{L}{2}(\dot{Q}_1^2+\dot{Q}_2^2+\dot{Q}_3^2)-\frac{1}{2C}(Q_1^2+Q_2^2+Q_3^2)+\frac{1}{2}\left(\int\dot{Q}_1^2 R_1 dt\right.$$
$$\left.+\int\dot{Q}_2^2 R_2 dt+\int\dot{Q}_3^2 R_3 dt\right)-M_{21}\dot{Q}_1\dot{Q}_2-M_{31}\dot{Q}_1\dot{Q}_3+Q_1 V_{in}(t) \tag{6}$$

A Ratio of *D*=30 nm to *D*=0 nm
B Ratio of *D*=60 nm to *D*=0 nm
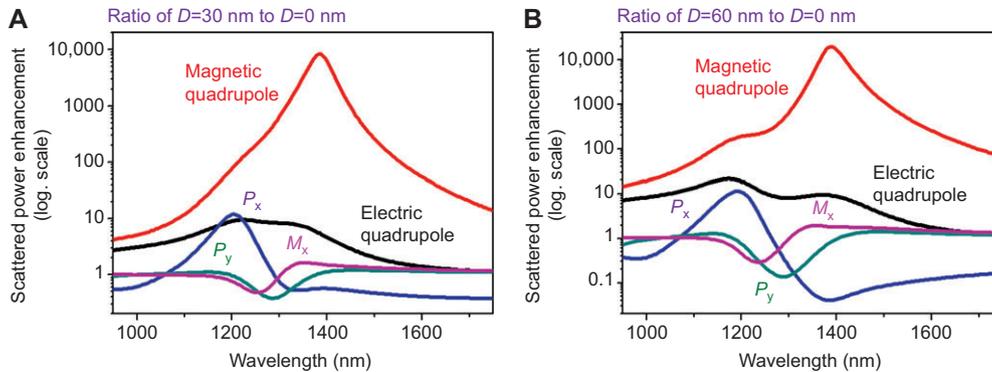
Figure 5 Ratio of scattered power by electric and magnetic multipoles with (A) *D*=30 nm and (B) *D*=60 nm related to *D*=0 nm.
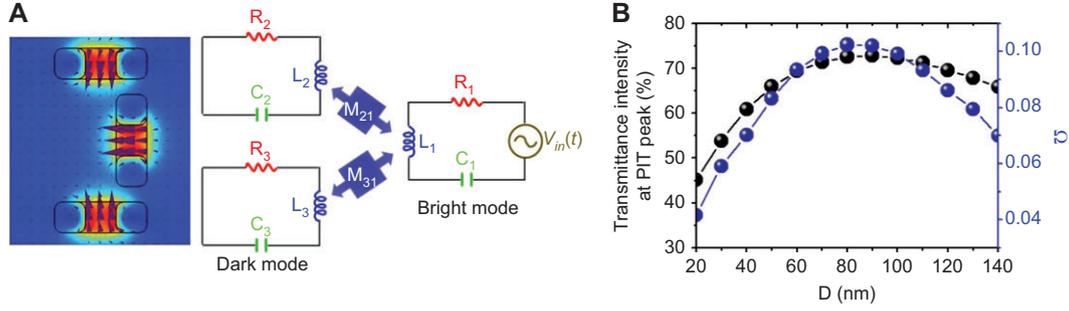
Figure 6 (A) Left: simulation result of magnetic field intensity (color-coded) and direction of magnetic field (purple arrows) in the case of D=60 nm. Right: Corresponding RLC circuits employed to investigate the coupling strength between bright and dark elements. (B) Black curve: transmittance intensity at PIT peak extracted by FEM simulation. Blue curve: fitting parameter Ω based on RLC circuits.

where, $I_i(t)=dQ_i(t)/dt$, where i=1, 2, 3 is the current flowing in the circuit i. Substituting Eq. (6) to the Euler-Lagrangian equations $\dfrac{d}{dt}\left(\dfrac{\partial \Gamma}{\partial \dot{Q}_i}\right)-\dfrac{\partial \Gamma}{\partial Q_i}=0$, (i=1, 2, 3), we obtain three coupled differential equations,

$$\frac{dI_1}{dt}+\gamma_1 I_1+\omega_0^2 Q_1-\Omega_{21}\frac{dI_2}{dt}-\Omega_{31}\frac{dI_3}{dt}=Ve^{-i\omega t} \quad (7)$$

$$\frac{dI_2}{dt}+\gamma_2 I_2+(\omega_0+\delta)^2 Q_2-\Omega_{21}\frac{dI_1}{dt}=0 \quad (8)$$

$$\frac{dI_3}{dt}+\gamma_3 I_3+(\omega_0+\delta)^2 Q_3-\Omega_{31}\frac{dI_1}{dt}=0 \quad (9)$$

Here, $\gamma_i=R_i/L$ (i=1, 2, 3) is the energy dissipation of each circuit, $\omega_0^2=1/LC$ is the resonant frequency associated with an isolated U-shaped SRR. $\Omega_{i1}=M_{i1}/L$ (i=2, 3) is the coefficient that describes the coupling intensity between the bright (VSRR) and dark (HSRR) circuits. Because of the same vertical distance between VSRR and each of the HSRRs, the induced surface currents I_2 and I_3 are identical, similarly, $\Omega_{21}=\Omega_{31}=\Omega$. A detuning parameter δ is introduced to take into account of the resonant frequency shift as a result of the weak near-field coupling between the HSRR pair. Due to the opposing current flow in the HSRR pair, the damping factors in HSRRs (γ_2 and γ_3) should satisfy $\gamma_2\approx\gamma_3<<\gamma_1<<\omega_0$.

Subsequently, the energy dissipation as a function of frequency can be obtained by solving the Eqs. (7), (8) and (9):

$$P(\omega)=\frac{V^2}{L}\frac{i\omega\cdot[\omega^2+i\omega\gamma_2-(\omega_0+\delta)^2]}{(\omega^2+i\omega\gamma_1-\omega_0^2)[\omega^2+i\omega\gamma_2-(\omega_0+\delta)^2]-2\Omega^2\omega^4} \quad (10)$$

The results calculated using Eq. (10) are shown in Figure 3B as red-dotted curves with δ, γ_1 and γ_2 taken as fitting parameters to reproduce the simulation results where the detuning parameter δ is approximately 1.6 THz and γ_1 and γ_2 are roughly 35.8 THz and 20.5 THz, respectively. These values provide evidence to support our expectation of loss reduction in the HSRR pair because of the anti-parallel magnetic dipoles induced in the pair.

For enhancing the near-field coupling between the VSRR and HSRRs, the structural asymmetry must be introduced. However, not only the near-field coupling but the lateral distance between VSRR and HSRRs will be increased by introducing the structural asymmetry. Due to the near-field depending strength between plasmonic metamaterials strongly depend on the distance between each other, there will be a threshold of distance parameter D to generate the largest transmittance intensity at PIT peak. It will provide more practical applications based on the PIT characterizations so the evolution of PIT spectra can be better understood. Therefore, in order to gain a deeper realization of the evolution of the PIT spectra, the PIT transmission intensity peak as a function of the distance parameter D from 20 nm to 140 nm is shown in Figure 6B (black curve with spherical dots) for investigation. As expected, the intensity of transmittance peak increases initially with D, because the asymmetry allowed for coupling between VSRR and HSRRs. Further increase of D beyond a critical point near 80 nm actually leads to a decrease of the PIT transmittance because of the reduced coupling strength as a result of the separation increase, which is reflected by the coupling parameter Ω also shown in Figure 6B (blue curve with spherical dots).

Conclusions

A plasmon induced transparency in three-dimensional photonic metamolecules based on magnetic interaction has been demonstrated and investigated in the optical region. The excitation of such a magnetic quadrupole is a result of the fundamental electromagnetic theorem (Lenz's law) which indicates that it will induce a magnetic field to oppose the change in magnetic flux. Because of the particular orientation of erected U-shaped SRRs, the strong magnetic dipolar interaction between them provides multiple pathways for near-field coupling in plasmonic metamolecules by introducing structural asymmetry. Using numerical simulation, we have proved that destructive interference takes place between different excited pathways of bright and dark elements which leads to the observed PIT phenomenon. Furthermore, to generate the maximum transmittance intensity in PIT spectra, the lateral

distance between bright and dark modes is also a key factor that needs to be considered carefully. Without the proper distance between bright and dark modes, the PIT phenomenon is very difficult to observe even when the introducing structural asymmetry is very strong. This study of optical properties associated with magnetic resonance will provide important insight towards practical applications using magnetic plasmon material [30, 31, 34, 44, 45].

Acknowledgments

References

[1] Smith DR, Pendry JB, Wiltshire MCK. Metamaterials and negative refractive index. Science 2004;305:788–92.

[2] Shalaev VM. Optical negative-index metamaterials. Nat Photon 2007;1:41–48.

[3] Huang Y-W, Chen WT, Wu PC, Fedotov V, Savinov V, Ho YZ, Chau Y-F, Zheludev NI, Tsai DP. Design of plasmonic toroidal metamaterials at optical frequencies. Opt Express 2012;20:1760–68.

[4] Kaelberer T, Fedotov VA, Papasimakis N, Tsai DP, Zheludev NI. Toroidal dipolar response in a metamaterial. Science 2010;330:1510–12.

[5] Fang N, Lee H, Sun C, Zhang X. Sub-diffraction-limited optical imaging with a silver superlens. Science 2005;308:534–37.

[6] Ozaki M, Kato J-i, Kawata S. Surface-plasmon holography with white-light illumination. Science 2011;332:218–20.

[7] Maksymov I, Staude I, Miroshnichenko AE, Kivshar YS. Optical Yagi-Uda nanoantennas. Nanophotonics 2012;1:65–81.

[8] Kadic M, Guenneau S, Enoch S, Huidobro PA, Martín-Moreno L, García-Vidal FJ, Renger J, Quidant R. Transformation plasmonics. Nanophotonics 2012;1:51–64.

[9] Chang CM, Chu CH, Tseng ML, Huang YW, Huang HW, Chen BH, Huang DW, Tsai DP. Light manipulation by gold nanobumps. Plasmonics 2012;7:563–69.

[10] Chen WT, Wu PC, Chen CJ, Weng CJ, Lee H-C, Yen T-J, Kuan C-H, Mansuripur M, Tsai DP. Manipulation of multidimensional plasmonic spectra for information storage. Appl Phys Lett 2011;98:171106–3.

[11] Ly-Gagnon DS, Balram KC, White JS, Wahl P, Brongersma ML, Miller DAB. Routing and photodetection in subwavelength plasmonic slot waveguides. Nanophotonics 2012;1:9–16.

[12] Castelletto S, Li X, Gu M. Frontiers in diffraction unlimited optical methods for spin manipulation, magnetic field sensing and imaging using diamond nitrogen vacancy defects. Nanophotonics 2012;1:139–153.

[13] Yen TJ, Padilla WJ, Fang N, Vier DC, Smith DR, Pendry JB, Basov DN, Zhang X. Terahertz magnetic response from artificial materials. Science 2004;303:1494–96.

[14] Liu N, Liu H, Zhu SN, Giessen H. Stereometamaterials. Nat Photon 2009;3:157–62.

[15] Linden S, Enkrich C, Wegener M, Zhou JF, Koschny T, Soukoulis CM. Magnetic response of metamaterials at 100 terahertz. Science 2004;306:1351–53.

[16] Liu N, Guo HC, Fu LW, Kaiser S, Schweizer H, Giessen H. Three-dimensional photonic metamaterials at optical frequencies. Nat Mater 2008;7:31–37.

[17] Liu N, Mukherjee S, Bao K, Brown LV, Dorfmüller J, Nordlander P, Halas NJ. Magnetic plasmon formation and propagation in artificial aromatic molecules. Nano Lett 2011;12:364–69.

[18] Lapine M, Shadrivov IV, Powell DA, Kivshar YS. Magnetoelastic metamaterials. Nat Mater 2012;11:30–33.

[19] Chen WT, Chen C-J, Wu PC, Sun S, Zhou L, Guo G-Y, Hsiao CT, Yang K-Y, Zheludev NI, Tsai DP. Optical magnetic response in three-dimensional metamaterial of upright plasmonic metamolecules. Opt Express 2011;19:12837–42.

[20] Fan KB, Strikwerda AC, Tao H, Zhang X, Averitt RD. Stand-up magnetic metamaterials at terahertz frequencies. Opt Express 2011;19:12619–27.

[21] Chen CC, Hsiao CT, Sun S, Yang K-Y, Wu PC, Chen WT, Tang YH, Chau Y-F, Plum E, Guo G-Y, Zheludev NI, Tsai DP. Fabrication of three dimensional split ring resonators by stress-driven assembly method. Opt Express 2012;20:9415–20.

[22] Field JE, Hahn KH, Harris SE. Observation of electromagnetically induced transparency in collisionally broadened lead vapor. Phys Rev Lett 1991;67:3062–65.

[23] Boller KJ, Imamolu A, Harris SE. Observation of electromagnetically induced transparency. Phys Rev Lett 1991;66:2593–96.

[24] Garrido Alzar CL, Martinez MAG, Nussenzveig P. Classical analog of electromagnetically induced transparency. Am J Phys 2002;70:37.

[25] Harden J, Joshi A, Serna JD. Demonstration of double eit using coupled harmonic oscillators and rlc circuits. Eur J Phys 2011;32:541–58.

[26] Gallinet B, Martin OJF. Influence of electromagnetic interactions on the line shape of plasmonic fano resonances. ACS Nano 2011;5:8999–9008.

[27] Davis TJ, Gómez DE, Vernon KC. Simple model for the hybridization of surface plasmon resonances in metallic nanoparticles. Nano Lett 2010;10:2618–25.

[28] Zhang S, Genov DA, Wang Y, Liu M, Zhang X. Plasmon-induced transparency in metamaterials. Phys Rev Lett 2008;101:047401.

[29] Dong Z-G, Liu H, Cao J-X, Li T, Wang S-M, Zhu S-N, Zhang X. Enhanced sensing performance by the plasmonic analog of electromagnetically induced transparency in active metamaterials. Appl Phys Lett 2010;97:114101.

[30] Liu N, Weiss T, Mesch M, Langguth L, Eigenthaler U, Hirscher M, Sönnichsen C, Giessen H. Planar metamaterial analogue of electromagnetically induced transparency for plasmonic sensing. Nano Lett 2010;10:1103–07.

[31] Yannopapas V, Paspalakis E, Vitanov NV. Electromagnetically induced transparency and slow light in an array of metallic nanoparticles. Physical Review B 2009;80:035104.

[32] Papasimakis N, Zheludev NI. Metamaterial-induced transparency: Sharp fano resonances and slow light. Opt Photon News 2009;20:22–27.

[33] Davis TJ, Hentschel M, Liu N, Giessen H. Analytical model of the three-dimensional plasmonic ruler. ACS Nano 2012;6:1291–98.

[34] Liu N, Hentschel M, Weiss T, Alivisatos AP, Giessen H. Three-dimensional plasmon rulers. Science 2011;332:1407–10.

[35] Moser HO, Rockstuhl C. 3D Thz metamaterials from micro/nanomanufacturing. Laser & Photon Rev 2012;6:219-44.

[36] Soukoulis CM, Wegener M. Past achievements and future challenges in the development of three-dimensional photonic metamaterials. Nat Photon 2011;5:523–30.

[37] Liu N, Langguth L, Weiss T, Kästel J, Fleischhauer M, Pfau T, Giessen H. Plasmonic analogue of electromagnetically induced transparency at the drude damping limit. Nat Mater 2009;8:758–62.

[38] Artar A, Yanik AA, Altug H. Multispectral plasmon induced transparency in coupled meta-atoms. Nano Lett 2011;11:1685–89.

[39] Papasimakis N, Fedotov VA, Zheludev NI, Prosvirnin SL. Metamaterial analog of electromagnetically induced transparency. Phys Rev Lett 2008;101:253903.

[40] Lassiter JB, Sobhani H, Knight MW, Mielczarek WS, Nordlander P, Halas NJ. Designing and deconstructing the fano lineshape in plasmonic nanoclusters. Nano Lett 2011;12:1058–62.

[41] Maier SA, Brongersma ML, Kik PG, Meltzer S, Requicha AAG, Atwater HA. Plasmonics – a route to nanoscale optical devices. Adv Mater 2001;13:1501–05.

[42] Maier SA, Atwater HA. Plasmonics: Localization and guiding of electromagnetic energy in metal/dielectric structures. J Appl Phys 2005;98:011101–10.

[43] Liu N, Mukherjee S, Bao K, Li Y, Brown LV, Nordlander P, Halas NJ. Manipulating magnetic plasmon propagation in metallic nanocluster networks. ACS Nano 2012;6:5482–88.

[44] Chen J, Li Z, Yue S, Xiao J, Gong Q. Plasmon-induced transparency in asymmetric t-shape single slit. Nano Lett 2012;12:2494–98.

[45] Taubert R, Hentschel M, Kästel J, Giessen H. Classical analog of electromagnetically induced absorption in plasmonics. Nano Lett 2012;12:1367–71.